

PAPER

[View Article Online](#)
[View Journal](#) | [View Issue](#)Cite this: *Dalton Trans.*, 2021, **50**,
15274Modular synthesis of antimalarial quinoline-based
PGM metallarectangles†Taryn M. Golding,  Mziyanda Mbaba and Gregory S. Smith  *

A new ditopic, quinoline-based ligand **L** (7-chloro-4-(pyridin-4-yl)quinoline) was synthesized via a Suzuki cross-coupling reaction. The ligand was utilized to synthesize the corresponding half-sandwich iridium(III) and ruthenium(II) binuclear complexes (**1c** and **1d**) and the subsequent metallarectangles (**2c**, **2d**, **3c**, and **3d**), via [2 + 2] coordination-driven self-assembly. Single-crystal X-ray diffraction confirmed the proposed molecular structure of the binuclear complex $[(\text{IrCl}_2(\text{Cp}^*))_2(\mu\text{-L})]$ (**1c**) and DFT calculations were used to predict the optimized geometry of the rectangular nature of $[(\text{Ir}(\mu\text{-Cl})(\text{Cp}^*))_4(\mu\text{-L})_2](\text{CF}_3\text{SO}_3)_4$ (**2c**). All of the metallarectangles were isolated as their triflate salts and characterized using various spectroscopic (^1H , $^{13}\text{C}\{^1\text{H}\}$, DOSY NMR, and IR spectroscopy) and analytical techniques (ESI-MS). The synthesized compounds were screened against the NF54 chloroquine-sensitive (CQS) and K1 chloroquine-resistant (CQR) strains of *Plasmodium falciparum*. Incorporation of the ubiquitous quinoline core and metal complexation significantly enhanced the *in vitro* biological activity, with an increase in the nuclearity correlating with an increase in the resultant antiparasmodial activity. This was observed across both parasitic strains, alluding to the potential of supramolecular metallarectangles to act as antiparasmodial agents. Inhibition of haemozoin formation was considered a potential mechanism of action and selected metallarectangles exhibit β -haematin inhibition activity with near comparable activity to chloroquine.

Received 24th August 2021,
Accepted 3rd October 2021

DOI: 10.1039/d1dt02842a

rsc.li/dalton

Introduction

Malaria, an infectious mosquito-borne disease caused by a blood parasite of the genus *Plasmodium*, is associated with high levels of morbidity and mortality in adults and children and occurs throughout tropical and subtropical regions of the world.^{1–4} Despite the overall number of estimated cases declining between 2010 to 2014, subsequent years have seen a resurgence in malaria cases globally.¹ The World Health Organisation (WHO) estimated that in 2019 there were approximately 229 million cases of malaria worldwide.¹

The eventual recognition of quinoline-based antimalarials, such as chloroquine (CQ),⁵ provided new hope for the treatment of this disease. CQ quickly became the most effective and widely used antimalarial drug.⁵ Unfortunately, its efficacy has been greatly compromised by the advent of drug-resistant strains of *P. falciparum*.^{2,5} Despite this, the quinoline scaffold continues to be attractive for the design and synthesis of new antimalarial agents. Its limited host toxicity, cost-effective synthesis, ease of use, and excellent clinical efficiency⁶ have

prompted efforts to develop new antimalarial drugs based on this pharmacophoric unit (e.g. amodiaquine, mefloquine, etc.).² The WHO now recommends artemisinin-based combination therapy (ACT) as the standard first-line therapy for uncomplicated malaria caused by *P. falciparum*.¹ This treatment regimen involves administration of artemisinin, or a derivative thereof, followed by a second antimalarial, preferably with a different mechanism of action, to ensure complete parasite clearance. Despite the proven effectiveness of ACT, disadvantages associated with this treatment regimen include poor patient compliance, increased risk of adverse effects caused by drug-drug interactions, and elevated costs.^{7–9} Furthermore, even in combination, the individual drugs are also susceptible to the development of resistance, which has been emerging.^{2,10}

The intrinsic and acquired resistance to several chemotherapeutic agents renders drugs that were once highly efficacious, fruitless, hampering the drug development progress made thus far. This has prompted research into alternative approaches, to combat the rising resistance. One approach that is gaining impetus is the incorporation of metals and this has proven to be an invaluable strategy.^{11–14} This field was stimulated by the success of the metal-based anticancer drug cisplatin.^{15,16} Since then, organometallic complexes as antimalarial agents have also generated significant scientific interest,¹⁷ exemplified by the antimalarial ferroquine (FQ).^{2,18} Due

Department of Chemistry, University of Cape Town, Rondebosch, Cape Town, South Africa. E-mail: gregory.smith@uct.ac.za

† Electronic supplementary information (ESI) available. CCDC 2089889 (**1c**). For ESI and crystallographic data in CIF or other electronic format see DOI: 10.1039/d1dt02842a

to the emerging chemoresistance and the limited arsenal of effective antimalarial agents, metal complexes based on novel scaffolds offer an excellent opportunity to find new leads against this infectious disease.

Supramolecular coordination complexes (SCCs), formed *via* coordination-driven self-assembly, are discrete systems stabilized by non-covalent intermolecular interactions.^{19,20} The synthetic strategy for the spontaneous assembly of rectangular architectures requires a step-wise synthetic procedure.^{21–23} The first step toward their synthesis requires synthesizing a stable, pre-organized, bimetallic molecular clip.^{22–30} Compared to main group metals, transition metals are often utilized due to their well-defined and predictable coordination geometries.^{31,32} To ensure the formation of a discrete supramolecular architecture, directing ligands such as cyclopentadienyl and arene-based ligands are used to occupy concomitant coordination sites at the octahedral metal centre.^{19,21,22,32–34} Half-sandwich transition metal complexes are thus promising building blocks to generate metallacycles.^{24,31,33,35–39} A suitable bifunctional donor, which acts as a bridging ligand, can then coordinate predictably to generate a [2 + 2] rectangular 2-D architecture.^{22–30,37}

Over the years, metallamacrocyclic supramolecular complexes containing organometallic rhodium, ruthenium, and iridium half-sandwich fragments have received a considerable amount of attention due to their myriad of potential applications,⁴⁰ including as host-guest,^{41–43} and drug-delivery systems,^{44–47} and in catalysis.⁴⁸ Despite extensive research into the pharmacological activity of small metal-based compounds,

investigations into the pharmacological activity of metallo-supramolecular coordination compounds have primarily centred on their potential as novel anticancer agents (see selected examples in Fig. 1).^{27,36,49–65} The exploration into the use of such complexes for the treatment of alternative diseases is limited and warrants further exploration.

Herein we describe the synthesis and characterisation of a series of iridium(III) and ruthenium(II) metallarectangles, containing a new 7-chloro-4-(pyridin-4-yl)quinoline-based ligand. To the best of our knowledge, no studies have explored the antimalarial properties of metallarectangles. Consequently, the metallarectangles prepared in this study were evaluated against the chloroquine-sensitive (CQS) NF54 and chloroquine-resistant (CQR) K1 strains of *P. falciparum*. This study also explored the β -haematin inhibition ability of selected metallarectangles, as a potential mechanism of action.

Results and discussion

Synthesis and characterisation

The synthesis of the ditopic quinoline-containing ligand **L**, the corresponding binuclear complexes (**1c** and **1d**) and the subsequent metallarectangles (**2c**, **2d**, **3c**, and **3d**) is outlined in Scheme 1. The known prototypical complexes (**1a**, **1b**, **2a**, **2b**, **3a**, **3b**) containing the bipyridyl ligand were also prepared and evaluated alongside the quinoline-based complexes (*vide infra*, Table 1). The synthesis of the ligand (**L**) proceeded *via* a Suzuki cross-coupling reaction, following a modified literature

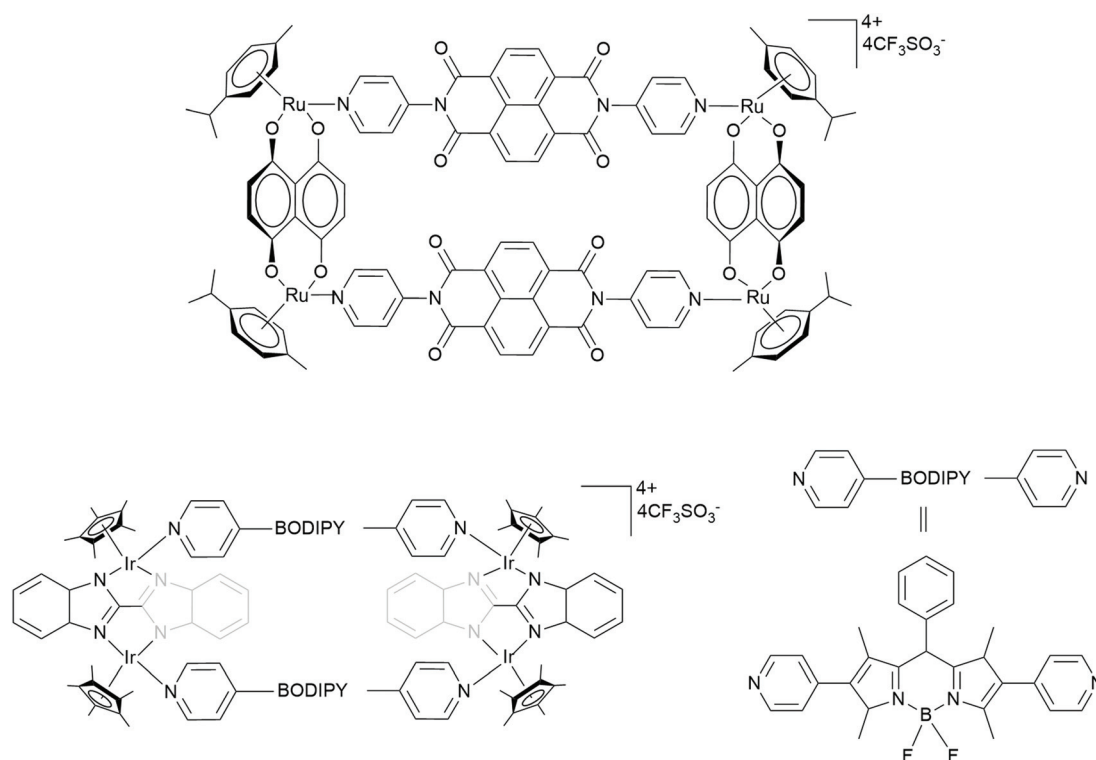
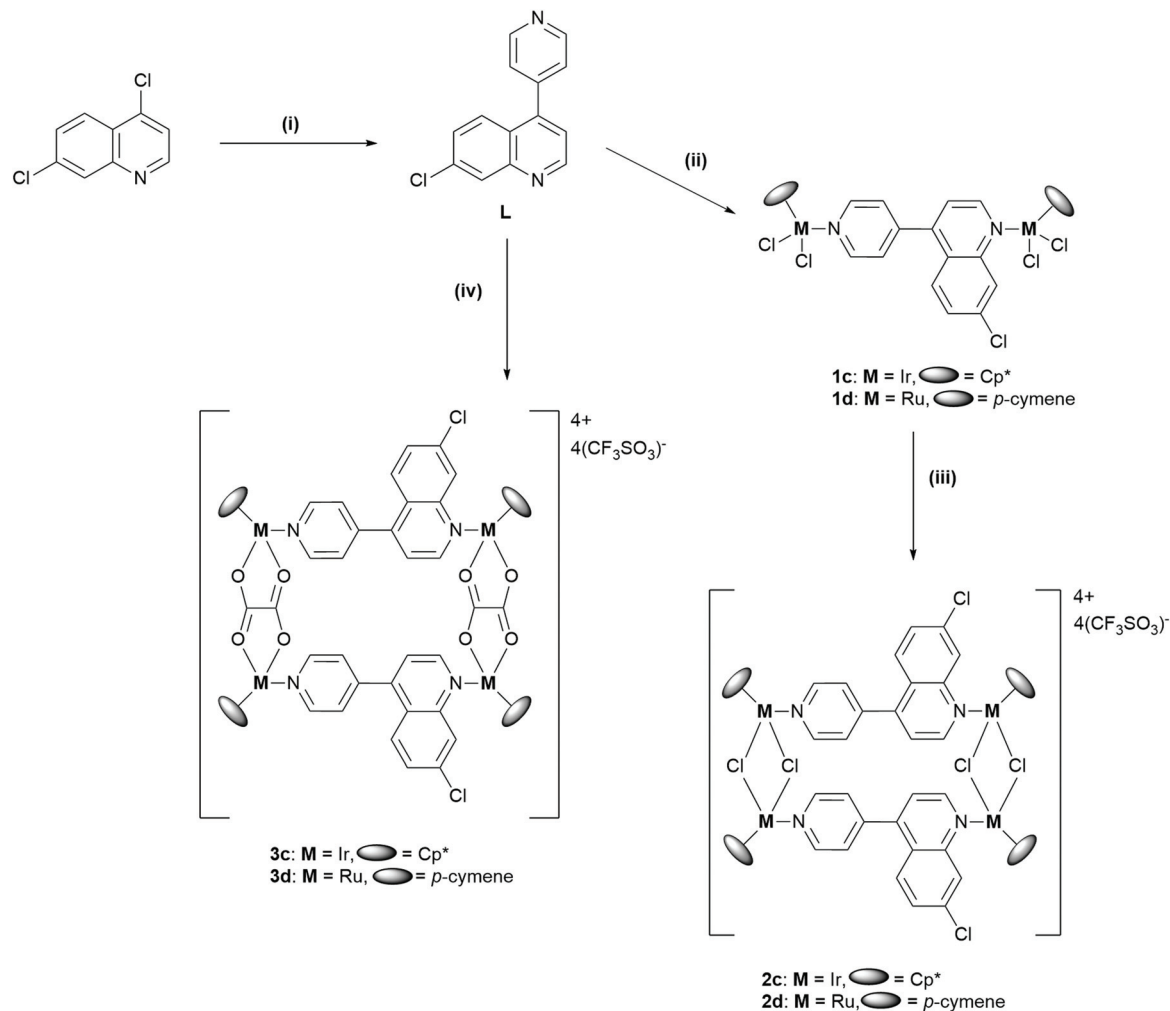


Fig. 1 Selected examples of metallarectangles displaying potent anticancer cytotoxic activity against selected cancer cell lines.^{27,53}





Scheme 1 Synthesis of ditopic quinoline-containing ligand (L) and the corresponding iridium(III) and ruthenium(II) binuclear complexes (**1c** and **1d**) and metallarectangles (**2c**, **2d**, **3c**, and **3d**). Reagents and conditions: (i) 4-pyridylboronic acid (1.1 eq.), Pd(OAc)₂ (0.01 eq.), PCy₃ (0.024 eq.), K₃PO₄ (1.7 eq.), 1,4-dioxane, reflux, 18 h; (ii) [IrCp*(μ-Cl)Cl]₂ or [Ru(p-cymene)(μ-Cl)Cl]₂ (0.8 eq.), CH₂Cl₂, r.t., 6 h; (iii) AgCF₃SO₃ (2.0 eq.) in CH₃CN, CH₂Cl₂, r.t., 24 h; (iv) [{IrCl(Cp*)}₂(μ-η²-η²-C₂O₄)] or [{RuCl(p-cymene)₂(μ-η²-η²-C₂O₄)] (1 eq.), AgCF₃SO₃ (2.0 eq.) in CH₃CN, CH₃OH, r.t., 24 h.

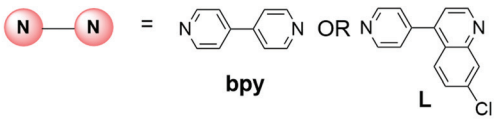
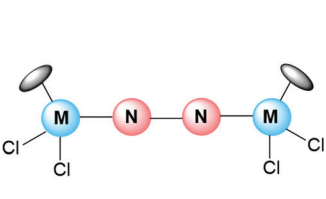
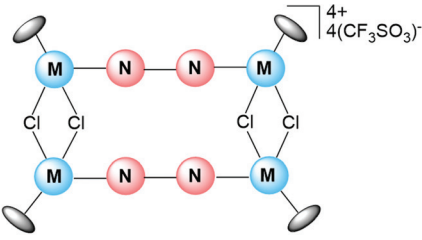
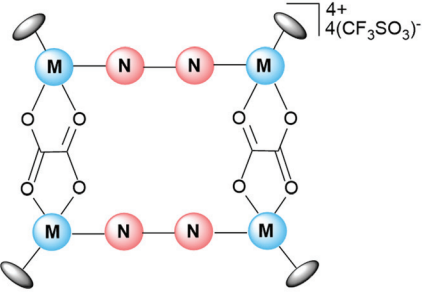
method by Kudo *et al.*,⁶⁶ yielding the desired compound as a white crystalline powder in a moderate yield of 42%. The synthesis of the iridium(III) and ruthenium(II) binuclear complexes (**1c** and **1d** respectively) were achieved *via* a bridge-splitting reaction of the appropriate dimer, allowing for insertion of the *N,N'*-ditopic ligand, and subsequent coordination to both nitrogen donor atoms. The resultant complexes (**1c** and **1d**) were isolated in excellent yields (74–76%), as yellow powders. The tetranuclear iridium(III) and ruthenium(II) metallarectangles, [{Ir(μ-Cl)(Cp*)}₄(μ-L)₂](CF₃SO₃)₄ (**2c**) and [{Ru(μ-Cl)(p-cymene)₄(μ-L)₂](CF₃SO₃)₄ (**2d**) (L = 7-chloro-4-(pyridin-4-yl)quinoline), were prepared from the binuclear complexes [{IrCl₂(Cp*)}₂(μ-L)] (**1c**) and [{RuCl₂(p-cymene)₂(μ-L)] (**1d**), *via* coordination-driven self-assembly, and isolated as their triflate salts. Metallarectangles **3c** and **3d**, containing chelating oxalato-ligands, were synthesized by reacting either [{IrCl(Cp*)}₂(μ-η²-η²-C₂O₄)] or [{RuCl(p-cymene)₂(μ-η²-η²-C₂O₄)] with silver trifluoromethanesulfonate, ensuring complete abstrac-

tion of the chlorides. Thereafter, the addition of ligand L resulted in coordination at the vacant coordination sites, and the resultant complexes (**3c** and **3d**) formed *via* coordination-driven self-assembly. All of the metallarectangles displayed excellent solubility in CH₂Cl₂ and DMSO and were insoluble in a range of non-polar organic solvents, such as Et₂O, hexane, pentane, and toluene. The ligand L and all the metal complexes were characterized using ¹H NMR and ¹³C{¹H} NMR spectroscopy, IR spectroscopy, and electrospray ionization mass spectrometry (ESI-MS). The metallarectangles (**2c**, **2d**, **3c**, and **3d**) were further analyzed using Diffusion-Ordered Spectroscopy (DOSY) to confirm the presence of a single entity in solution.

Spectroscopic details of the ligand L and the corresponding binuclear complexes (**1c** and **1d**) are provided in the ESI (Fig. S1–S7†). Analysis of the ¹H NMR spectrum of the tetracationic iridium(III) metallarectangle **2c**, confirms coordination to both nitrogen atoms of the unsymmetrical ligand L



Table 1 *In vitro* antiplasmodial activity of 4,4'-bipyridine, ligand **L**, and the corresponding binuclear complexes (**1a–1d**) and metallarectangles (**2a–2d** and **3a–3d**) against the CQS (NF54) and CQR (K1) strains of *P. falciparum*

			
			
			
			
<p> 1a: M = Ir, Cp* = Cp*, N,N = bpy 1b: M = Ru, Cp* = <i>p</i>-cymene, N,N = bpy 1c: M = Ir, Cp* = Cp*, N,N = L 1d: M = Ru, Cp* = <i>p</i>-cymene, N,N = L </p> <p> 2a: M = Ir, Cp* = Cp*, N,N = bpy 2b: M = Ru, Cp* = <i>p</i>-cymene, N,N = bpy 2c: M = Ir, Cp* = Cp*, N,N = L 2d: M = Ru, Cp* = <i>p</i>-cymene, N,N = L </p> <p> 3a: M = Ir, Cp* = Cp*, N,N = bpy 3b: M = Ru, Cp* = <i>p</i>-cymene, N,N = bpy 3c: M = Ir, Cp* = Cp*, N,N = L 3d: M = Ru, Cp* = <i>p</i>-cymene, N,N = L </p>			
Compound	IC ₅₀ (μM) ± SE NF54	IC ₅₀ (μM) ± SE K1	Resistance index (RI) ^a
Ligands			
4,4'-Bipyridine	500.50 ± 35.01	778.76 ± 12.68	1.6
L	50.88 ± 7.34	118.31 ± 5.97	2.3
Binuclear complexes			
1a	90.66 ± 5.06	211.97 ± 1.99	2.3
1b	13.33 ± 4.21	15.54 ± 0.46	1.2
1c	46.26 ± 2.82	50.24 ± 0.16	1.1
1d	14.75 ± 1.05	17.39 ± 1.92	1.2
Metallarectangles			
2a	19.40 ± 0.73	17.14 ± 7.43	0.9
2b	9.41 ± 2.81	19.76 ± 1.29	2.1
2c	9.28 ± 0.75	15.30 ± 2.60	1.6
2d	ND ^b	ND ^b	
3a	26.25 ± 5.98	70.32 ± 1.26	2.7
3b	1.08 ± 0.53	2.25 ± 0.82	2.1
3c	20.55 ± 5.60	22.69 ± 5.38	1.1
3d	9.82 ± 0.89	7.65 ± 0.77	0.8
CQDP	0.0134 ± 0.00096	0.296 ± 0.0283	22.1

^a (IC₅₀ K1/IC₅₀ NF54). ^b ND = not determined.

(Fig. S11†). Two singlets at 1.74 and 1.64 ppm are assigned to the methyl protons of the four Cp* ligands, a consequence of the unsymmetrical nature of ligand **L**. The remaining aromatic proton signals collectively confirm the incorporation of two **L** ligands per molecule. The NMR spectrum of compound **2c** points to the formation of one pure complex. However, it is important to note the existence of one of four possible isomers as illustrated using **2c** as an example (Fig. 2). Based on the spectrum of complex **2c** (Fig. S11†), one can deduce that a single, symmetrical isomer is favoured, and thus any of the pure compounds, **A–D** (Fig. 2), could have formed. A mixture of conformational isomers would result in the coalescence of signals, as attested to by variable-temperature (VT) NMR spectroscopic analysis. It is postulated that the absence of observable conformational isomers, or rotamers, may be due to a high

barrier to rotation, resulting in restricted rotation. The reason for the selectivity toward a single constitutional isomer, however, is not entirely known, although steric strain may have a role to play.

In the ¹H NMR spectra of metallarectangles **2d** (Fig. S12†) and **3c** (Fig. S13†), each dominant signal is accompanied by a smaller set of signals. These spectra suggest the presence of conformational isomers, which was confirmed by VT-NMR analysis. The relative integrations confirm the presence of only two ligands (**L**) and four metal centres, and thus the formation of the desired metallarectangles (**2d** and **3c**). The ¹H NMR of metallarectangle **3d** (Fig. S14†), however, shows an apparent “doubling-up” of both the ligand **L** and *p*-cymene signals. VT-NMR analysis did not result in a coalescence of signals and it is thus speculated that the sample contains a mixture of two

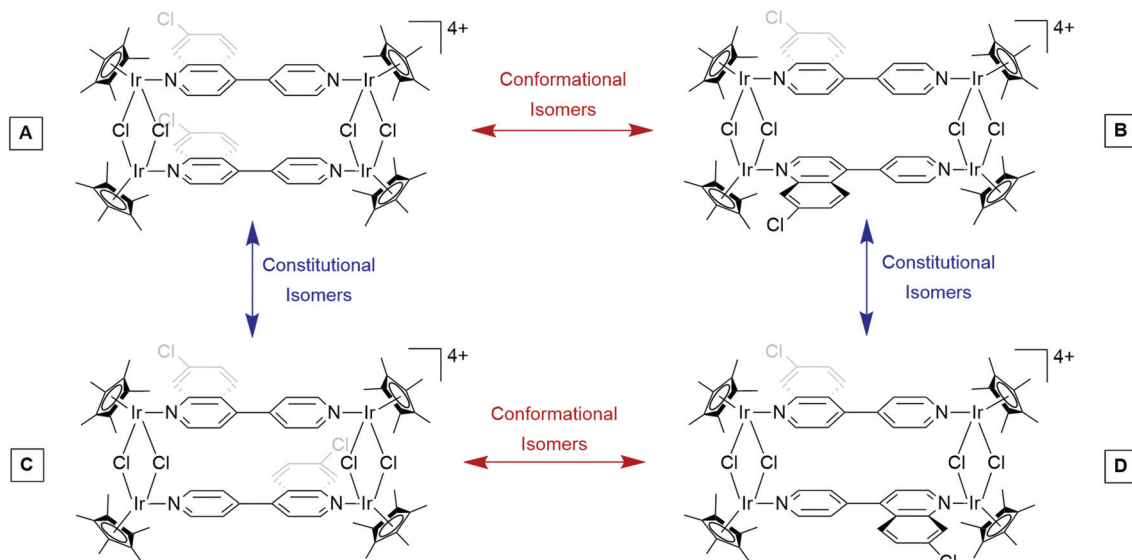


Fig. 2 Possible isomers of metallarectangle **2c**.

constitutional isomers. This is further supported by the presence of two sets of signals corresponding to ligand **L** in a 1 : 1 ratio. Moreover, the relative integrations to the *p*-cymene signals support the presence of two metallarectangles.

To further support these assertions, diffusion-ordered NMR (DOSY) spectra of metallarectangles **2c**, **2d**, **3c**, and **3d** were also recorded (Fig. S19–S22†) and the presence of a single diffusion line confirms the presence of a single discrete compound in solution. It should also be noted that although the ^1H NMR spectra of metallarectangles **2c**, **3c**, and **3d** reveal the presence of either conformational or constitutional isomers, the DOSY spectra still reveals a single vertical trace, as the isomers, despite being chemically different, have the same molecular weight and shape. This excludes the formation of unwanted side-products such as polymers.

For the metallarectangles $[\{\text{Ir}(\mu\text{-Cl})(\text{Cp}^*)\}_4(\mu\text{-L})_2](\text{CF}_3\text{SO}_3)_4$ (**2c**) and $[\{\text{Ru}(\mu\text{-Cl})(p\text{-cymene})\}_4(\mu\text{-L})_2](\text{CF}_3\text{SO}_3)_4$ (**2d**), IR spectroscopy reveals $\nu(\text{C}=\text{N})$ stretching vibrations at 1610 and 1589 cm^{-1} attributed to the two different $\text{C}=\text{N}$ functionalities, $\text{C}=\text{N}_{\text{py}}$ and $\text{C}=\text{N}_{\text{quin}}$, respectively. For the complexes $[\{\text{Ir}(\text{Cp}^*)\}_4(\mu\text{-}\eta^2\text{-}\eta^2\text{-C}_2\text{O}_4)(\mu\text{-L})_2](\text{CF}_3\text{SO}_3)_4$ (**3c**) and $[\{\text{Ru}(p\text{-cymene})\}_4(\mu\text{-}\eta^2\text{-}\eta^2\text{-C}_2\text{O}_4)(\mu\text{-L})_2](\text{CF}_3\text{SO}_3)_4$ (**3d**), the characteristic $\nu(\text{C}=\text{O})$ stretching vibration is observed at 1627 cm^{-1} , overlapping with the $\nu(\text{C}=\text{N})$ absorption bands. Furthermore, the infrared spectra of the metallarectangles (**2c**, **2d**, **3c**, and **3d**) (Fig. S23–S26†) are dominated by strong absorption bands at 1249 cm^{-1} (CF_3 *sym.*), 1223 cm^{-1} (SO_3 *asym.*), 1155 cm^{-1} (CF_3 *asym.*), and 1026 cm^{-1} (SO_3 *sym.*), due to the stretching vibrations of the triflate anions. These assignments are well documented in literature^{67–69} and support the formation of the cationic assemblies as their triflate salts. ESI-MS analysis further supports the formation of metallarectangles **2c**, **2d**, **3c**, and **3d**. The mass spectral data show tetracationic peaks for iridium metallarectangles **2c** (m/z 483.1129) and **3c** (m/z 492.0915), corresponding to the loss of four triflate counterions. The pres-

ence of these ion peaks, corresponding to the loss of one or more counter ions, is often observed for supramolecular rectangular architectures^{27,52–54} and correlates with the calculated values. Furthermore, dicationic peaks were observed for all iridium and ruthenium metallarectangles (**2c**, **2d**, **3c**, and **3d**), which correlate with the loss of two triflate ions, $[\text{M} - 2\text{CF}_3\text{SO}_3]^{2+}$.

Single-crystal X-ray diffraction

Single crystals of the precursor binuclear complex **1c** were grown by the slow evaporation of a saturated chloroform solution, and the molecular structure elucidated by single-crystal X-ray diffraction. From the ORTEP diagram of complex **1c** (Fig. 3), the ditopic ligand **L** is observed to bridge two iridium(III) metal centres, with each iridium(III) further coordinated to two chloride ligands and a η^5 -pentamethylcyclopentadienyl (Cp^*) ligand. It is also apparent that one of the Cp^* ligands is disordered, with refined site occupancy factors of 0.394(9) and 0.606(9). The complex adopts the well-known “three-legged piano-stool” structure which is commonly observed in many other half-sandwich rhodium, iridium, and ruthenium complexes.^{70–73}

Complex **1c** crystallizes in the $P\bar{1}$ space group with a triclinic system. Further crystallographic data and refinement parameters are summarised in Table S1.† Additionally, selected bond lengths and angles are listed in Table S2.† The data in Table S2† suggests that the geometry around the iridium metal centre is pseudo-tetrahedral, as the bond angles around the metal centre range between 83.0° and 90.4° . Furthermore, the $\text{Ir}_1\text{-N}_1$ bond length ($2.113(6)\text{ \AA}$) is comparable to related iridium(III)-pyridyl complexes,^{28,30,53,72} however, the $\text{Ir}_{2A}\text{-N}_2$ and $\text{Ir}_{2B}\text{-N}_2$ bond lengths are slightly longer.^{28,30,53} Finally, the quinoline and pyridyl ring systems are not coplanar, as expected, with a torsion angle of 44.3° .



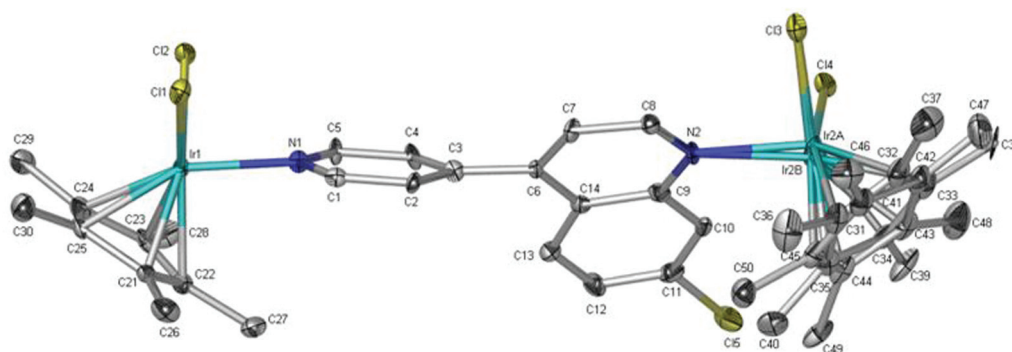


Fig. 3 Molecular structure of the iridium(III) binuclear complex **1c**. Solvent molecules (5-CHCl_3) and hydrogen atoms have been omitted for clarity. Ellipsoids are shown at 30% probability level.

Density functional theory (DFT) calculations

A theoretical structure indicative of the 2D-rectangular nature of complex **2c** is shown in Fig. 4, as determined from a density functional theory (DFT) geometry optimization. Similar to the molecular structure obtained for the binuclear complex **1c** (Fig. 3), the optimized structures shown in Fig. 4 also reveal a torsion angle between the pyridyl and quinoline ring systems of ligand **L**. Within the *syn*-complex, the torsion angles within the two ligands are 41.48° and 41.43° . Within the *anti*-complex, these angles are slightly smaller, with values of 33.33° and 34.70° . More notably, however, within a given isomer (*syn* or *anti*), the torsion angles within the two coordinated ligands are almost identical, suggesting that if one ring system (*e.g.* pyridyl or quinoline) rotates, the ring system directly opposite will rotate in a similar manner, possibly to relieve steric strain. This phenomenon is reported in the literature.⁷⁴ Furthermore, analysis of these structures reveals that the geometry around the iridium(III) metal centre is pseudo-tetrahedral, with bond angles ranging between 81.00° and 94.55° .

In vitro antiparasmodial assays

4,4'-Bipyridine, the new quinoline-containing ligand **L**, the corresponding binuclear complexes (**1a–1d**) and the metallarectangles (**2a–2d** and **3a–3d**) were evaluated for their *in vitro*

antiplasmodial activity against the CQS NF54 and the CQR K1 strains of *P. falciparum*. The biological results for the ligands and corresponding complexes are summarised in Table 1, with chloroquine diphosphate (CQDP) used as the control drug in this study.

Most notably, the antiparasmodial results reveal that the quinoline-containing analogues generally show superior activity in comparison with their corresponding prototypical 4,4'-bipyridyl congeners. The activity of the quinoline-containing ligand **L** (IC_{50} value = $50.88\ \mu\text{M}$) in the NF54 strain, outperforms 4,4'-bipyridine ($p = 0.03$) by almost 10-fold, pointing to the pharmacological benefits of incorporating a pharmacophoric quinoline scaffold into the framework of a potential drug candidate, as is exemplified in many antimalarial drugs.^{6,75,76} Furthermore, the activity of both ligands are generally enhanced upon metal complexation (statistically significant, $p < 0.05$), with most complexes approximately five-fold more potent than their respective ligands. Interestingly, the antiparasmodial activity further increases with an increase in nuclearity. For example, the IC_{50} value of 4,4'-bipyridine is $500.50\ \mu\text{M}$, however, upon complexation to form a binuclear complex (*e.g.* **1a**), the activity is increased five-fold. Formation of the corresponding metallarectangles (**2a** or **3a**) results in a further increase in activity by approximately four-fold. This trend was similarly observed for the ruthenium-bipyridyl analogues, as well as the quinoline congeners, further underpinning the

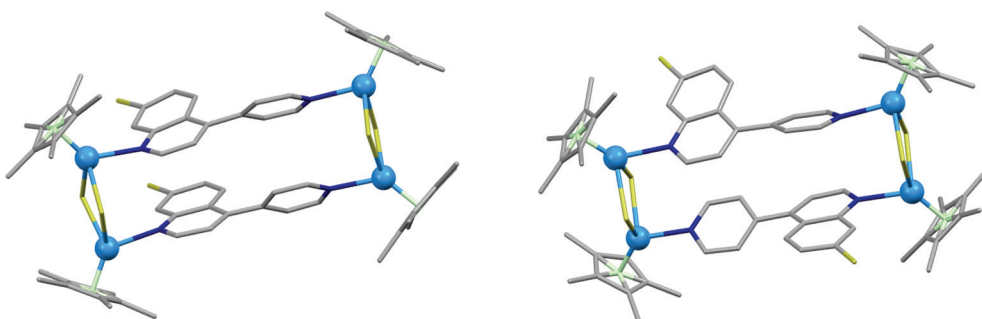


Fig. 4 DFT-optimized computational structure models of the *syn*- and *anti*-structures of metallarectangle **2c**.



plethora of studies that emphasize the advantages of metal incorporation on the pharmacological activity of organic compounds.^{72,77–79} Interestingly, the enhanced activity observed for the supramolecular metallarectangles demonstrates the potential of such multinuclear, highly charged systems, to act as antiplasmodial agents. The increased antiplasmodial activity observed upon complexation suggests that the metal centre may be crucial in reducing the parasitic viability, although the exact mechanism is still unclear. Stability studies demonstrate that most of the complexes are stable as attested to by ¹H NMR experiments, except for **3d** with small changes observed over the analogous incubation time. The most active complexes containing ligand **L** are metallarectangles **2c** and **3d**, with comparable activity (IC_{50} values of 9.28 and 9.82 μ M, respectively), although not as active as the clinical drug CQDP, which has an IC_{50} value of 0.0134 μ M in the NF54 strain.

The inhibitory data of the compounds tested against the multi-drug resistant K1 strain resembles the trend observed for the NF54 strain. The quinoline-containing ligand **L** was observed to be approximately seven-times more active than 4,4'-bipyridine, reiterating the importance of the pharmacophoric scaffold for antiplasmodial activity. The inhibitory data for the resistant strain similarly reveals that complexation enhances the antiplasmodial activity. Of the synthesized quinoline-containing compounds, metallarectangle **3d** showed the greatest activity, with an IC_{50} value in the low-micromolar range (IC_{50} = 7.65 μ M). Despite the moderate activity of the synthesized compounds, the observed antiplasmodial data is promising, as it points to a potentially new class of metal-based antiplasmodial agents and lends credence to the incorporation of the quinoline scaffold.

The resistance indices (RI) were, in most cases, slightly greater than 1, suggesting that the compounds are likely to experience some cross-resistance, albeit not to the same extent as CQ (RI = 22.1). Notably, the RI values of the quinoline-containing complexes (**1c**, **1d**, **2c**, **3c**, and **3d**), which range between 0.8–1.6, are lower than the RI value observed for the uncoordinated ligand **L** (RI = 2.3). This suggests that metal incorporation imposes a potentially new mechanism of action, which is not subject to the same resistance mechanism experienced by the uncoordinated ligand, minimizing cross-resistance.

β -Haematin inhibition studies

During the intraerythrocytic stage of the parasites' life cycle, the parasite degrades haemoglobin (Hb) found within the infected red blood cells of the host.^{80–82} A side product of this Hb digestion is the production of haem, which is toxic to the parasite. To circumvent these effects, the parasite initiates a detoxification mechanism, converting the free haem into inert crystalline haemozoin, which is non-toxic to the parasite.⁸¹ Many researchers have thus exploited this process by developing antimalarials that interfere with this haem detoxification method, the most promising of which has been chloroquine.^{5,83} Like chloroquine, the target for many amino-

quinoline-based antimalarials is the inhibition of haemozoin formation.^{2,82,84}

The presence of the quinoline scaffold in ligand **L**, and the corresponding complexes, prompted investigation into the β -haematin (synthetic haemozoin) inhibition ability of selected compounds, as a potential mechanism of action. The ability of a potential drug candidate to inhibit haemozoin formation can be measured using the NP-40 detergent-mediated β -haematin inhibition assay.^{85,86} Representative compounds (**L**, **3c**, and **3d**) were tested for their ability to inhibit β -haematin formation and the log-based dose-response curves are shown in Fig. 5. The compounds were screened in either duplicate or triplicate and the amount of synthetic haemozoin formed was quantified using the colorimetric pyridine ferrochrome method published by Egan *et al.*⁸⁷

Metallarectangle **3d**, which shows the most promising antiplasmodial activity across both strains, metallarectangle **3c**, the analogous iridium complex, and ligand **L**, were tested for their ability to inhibit β -haematin formation. Surprisingly, of the tested compounds, the quinoline-containing ligand **L** did not show any appreciable β -haematin inhibitory activity. Metallarectangles **3c** and **3d**, however, were found to inhibit β -haematin formation to almost the same extent as CQ, as indicated by their characteristic log-based sigmoidal curves (Fig. 5). The polyaryl nature of these complexes (**3c** and **3d**) suggests that they are capable of intermolecular π - π interactions and it may be possible that these complexes inhibit β -haematin formation through π - π stacking with haematin. The β -haematin inhibition activity of complexes **3c** and **3d** were, however, unexpected since ligand **L** did not demonstrate any β -haematin inhibitory activity. These results should not be read in isolation. Neither complexes **3c** nor **3d** show antiplasmodial activity comparable with CQ. However, the IC_{50} value of complex **3c** (IC_{50} = 28.29 μ M), obtained from the β -haematin inhibition assay, is fairly comparable with CQ (IC_{50} =

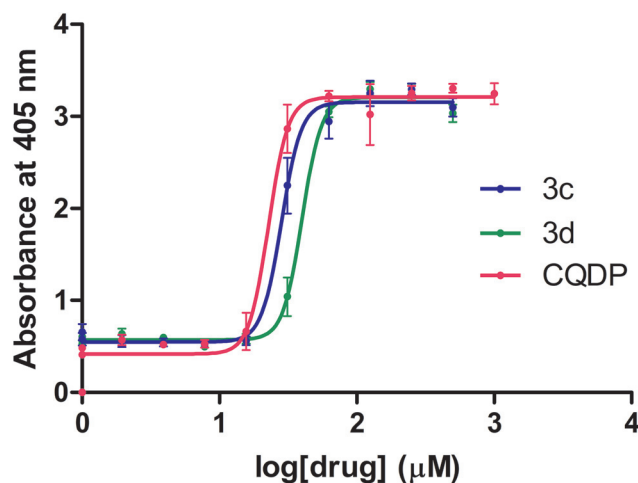


Fig. 5 Dose-response curves obtained for metallarectangles **3c** and **3d**, as well as CQDP, using the NP-40 detergent-mediated β -haematin inhibition assay.



22.75 μM). This suggests that complex **3c** is inhibiting β -haematin to almost the same extent as CQ, however, the observed *in vitro* antiparasmodial activities do not corroborate this finding. The results of this cell-free assay suggest that these compounds may be likely candidates for haemozoin inhibition in the parasite. However, other factors may be contributing to the limited *in vitro* antiparasmodial activity. One possibility is that entry into and/or accumulation in the parasitic DV, where haemozoin crystallization takes place, is limited possibly due to the highly charged nature and size of the assembly, as it has a very good cell-free β -haematin inhibitory activity but poor *in vitro* antiparasmodial activity.

Conclusions

A new quinoline-containing ditopic ligand (**L**) was prepared, successfully incorporating the ubiquitous quinoline pharmacophore, with the targeted ligand **L** mimicking the orthodox 4,4'-bipyridine ligand often used in the construction of metallarectangles. The quinoline-based ligand **L** was reacted with either $[\text{IrCl}(\mu\text{-Cl})(\text{Cp}^*)]_2$ or $[\text{RuCl}(\mu\text{-Cl})(p\text{-cymene})]_2$ to afford the precursor iridium(III) and ruthenium(II) binuclear complexes (**1c** and **1d**), which were further treated with silver triflate and, *via* coordination-driven self-assembly, formed the concomitant metallarectangles **2c** and **2d**, containing bridging chlorides. In addition, ligand **L** was reacted with either $[\{\text{IrCl}(\text{Cp}^*)\}_2(\mu\text{-}\eta^2\text{-}\eta^2\text{-C}_2\text{O}_4)]$ or $[\{\text{RuCl}(p\text{-cymene})\}_2(\mu\text{-}\eta^2\text{-}\eta^2\text{-C}_2\text{O}_4)]$, to form metallarectangles **3c** and **3d**, containing bridging oxalato ligands, as their triflate salts.

Single-crystal X-ray diffraction confirmed the molecular structure of the precursor binuclear complex **2c** and inevitably corroborated the structure of the quinoline-containing ligand **L**. Due to the unsymmetrical nature of the ligand, upon formation of the metallarectangles, there is a possibility of forming constitutional isomers. Interestingly, the ^1H NMR spectra of metallarectangles **2c**, **2d**, and **3c**, reveal a single isomer in solution, suggesting increased selectivity toward a preferred configuration. The ^1H NMR spectrum of ruthenium metallarectangle **3d**, however, suggests a mixture of two metallarectangles (constitutional isomers) in solution.

The new ligand (**L**), the precursor complexes (**1c** and **1d**), the metallarectangles (**2c**, **2d**, **3c**, and **3d**), as well as the corresponding 4,4'-bipyridine analogues (**1a**, **1b**, **2a**, **2b**, **3a**, and **3b**) were evaluated for their *in vitro* antiparasmodial activity in the CQS NF54 and CQR K1 strains of *P. falciparum*. The presence of the pharmacophoric quinoline scaffold significantly enhanced the antiparasmodial activity, emphasising the importance of the quinoline pharmacophore. Metal complexation resulted in a further increase in activity, with enhanced biological activity observed with an increase in the nuclearity. The calculated resistance indices further suggest that the compounds may experience mild cross-resistance, however, not to the extent of CQ. Despite not being very potent antimalarial agents, the metallarectangles do indeed show promising antiparasmodial activity with the potential for further development

through fine-tuning and ligand modification. A reason for the limited activity may be due to the size and/or highly charged nature of these SCCs, which may impede their uptake and/or accumulation in the parasite, although further in-depth studies are required to verify this hypothesis.

The presence of the quinoline pharmacophore prompted investigation into the β -haematin inhibition ability of ligand **L** and selected metallarectangles (**3c** and **3d**). Both metallarectangles show β -haematin inhibitory activity, with the iridium metallarectangle (**3c**) having an IC_{50} value (28.29 μM) comparable with CQ (IC_{50} = 22.75 μM). The superior cell-free β -haematin inhibitory activity of metallarectangle **3c**, but limited *in vitro* antiparasmodial activity, supports the hypothesis that entry of this large, highly charged compound into the digestive vacuole of the parasite is hindered, as entry into the cell will make this compound a likely candidate for haemozoin inhibition, and thus a promising antimalarial agent.

Experimental

General details

All reagents and solvents were purchased from commercial sources (Sigma-Aldrich, Merck, and KIMIX) and were used without further purification. The iridium and ruthenium dimers, $[\text{IrCp}^*(\mu\text{-Cl})\text{Cl}]_2$ ⁸⁸ and $[\text{Ru}(p\text{-cymene})(\mu\text{-Cl})\text{Cl}]_2$ ⁸⁹ respectively, $[\{\text{IrCl}(\text{Cp}^*)\}_2(\mu\text{-}\eta^2\text{-}\eta^2\text{-C}_2\text{O}_4)]$,³⁰ $[\{\text{RuCl}(p\text{-cymene})\}_2(\mu\text{-}\eta^2\text{-}\eta^2\text{-C}_2\text{O}_4)]$ ⁹⁰ and compounds **1a**,³⁴ **1b**,⁹¹ **2a**,³⁴ **2b**, **3a**,³⁰ and **3b**⁹⁰ were synthesised following literature methods. All reactions were carried out under an inert argon atmosphere using standard Schlenk line techniques unless otherwise stated. Nuclear magnetic resonance (NMR) spectra were recorded on a Bruker XR600 MHz spectrometer (^1H at 599.95 MHz and $^{13}\text{C}\{^1\text{H}\}$ at 151.0 MHz), a Bruker Topspin GmbH (^1H at 400.22 MHz and $^{13}\text{C}\{^1\text{H}\}$ at 100.65 MHz) or a Varian Mercury 300 (^1H at 300.08 MHz) spectrometer. These were equipped with a Bruker Biospin GmbH casing and sample injector at 30 °C and tetramethylsilane (TMS) was used as the internal standard. Infrared (IR) spectroscopy was performed on a PerkinElmer Spectrum 100 FT-IR spectrometer using Attenuated Total Reflectance (ATR) with vibrations measured in units of cm^{-1} . High resolution (HR) electrospray ionisation mass spectrometry (ESI-MS) was performed on a Waters Synapt G2 QTOF mass spectrometer with data recorded using the positive mode. Melting points were obtained using a Büchi Melting Point Apparatus B-540 and are uncorrected.

Synthesis

Procedure for the synthesis of 7-chloro-4-(pyridine-4-yl)quinoline (L**).** To a mixture of 4,7-dichloroquinoline (2.00 g, 0.0101 mol), 4-pyridinylboronic acid (1.37 g, 0.0111 mol), PCy_3 (0.0680 g, 0.242 mmol) and $\text{Pd}(\text{OAc})_2$ (0.0232 g, 0.103 mmol), an aqueous solution of K_3PO_4 (1.27 M, 13.5 mL, 0.0172 mol) was added, followed by 1,4-dioxane (29.6 mL) and the mixture refluxed at 100 °C for 21 hours. The reaction mixture was filtered through a pad of silica gel, the filtrate concentrated



under reduced pressure, and the aqueous residue extracted with EtOAc (3 × 30.0 mL). The organic layers were combined, dried over anhydrous MgSO₄, filtered, and the crude product purified *via* column chromatography, using hexane:ethyl acetate as the eluent to yield compound **L** as a white crystalline solid. **Yield**: 42% (1.02 g, 4.25 mmol). **R_f**: 0.36 (100% EtOAc). **LC-MS**: (*m/z*) = 241.0 (100% purity, *M* + 1). **¹H NMR (300 MHz, [D₆]-DMSO)**: δ(ppm) = 9.04 (d, 1H, H_a, ³*J*_{H-H} = 4.4 Hz); 8.79 (dd, 2H, H_b, *J* = 4.4, 1.6 Hz); 8.20 (d, 1H, H_c, ⁴*J*_{H-H} = 2.2 Hz); 7.84 (d, 1H, H_d, ³*J*_{H-H} = 9.0 Hz); 7.67 (dd, 1H, H_e, ³*J*_{H-H} = 9.0 Hz, ⁴*J*_{H-H} = 2.2 Hz); 7.60 (dd, 2H, H_f, *J* = 4.4, 1.6 Hz); 7.57 (d, 1H, H_g, ³*J*_{H-H} = 4.4 Hz). **¹³C{¹H} NMR (100 MHz, [D₆]-DMSO)**: δ (ppm) = 151.2, 150.0, 148.4, 145.0, 144.3, 134.4, 128.1, 128.0, 127.1, 124.2, 123.8, 121.7; **IR (ATR)** (*ν*_{max}/cm⁻¹): 1604, 1580 (C=N); **M.P.** (°C): 156.5–157.1.

General procedure for the synthesis of binuclear complexes (1c and 1d). Ligand **L** (1.2 eq.) was added to a stirring solution of the appropriate dimer ([IrCp*(μ-Cl)Cl]₂ or [Ru(*p*-cymene)(μ-Cl)Cl]₂) (1 eq.) in CH₂Cl₂ (15.0 mL). The mixture was stirred at r.t. for 6 hours to ensure completion of the reaction, as confirmed by TLC analysis. The solution was concentrated and added to excess cold Et₂O. This resulted in the precipitation of the corresponding binuclear complex, which was filtered and washed with copious amounts of cold Et₂O.

[{IrCl₂(Cp*)}₂(μ-L)], (**1c**). [IrCp*(μ-Cl)Cl]₂ (0.100 g, 0.126 mmol) was reacted with **L** (0.0350 g, 0.146 mmol), yielding **1c** as a bright yellow powder. **Yield**: 76% (0.0985 g, 0.0949 mmol); **¹H NMR (300 MHz, CDCl₃)**: δ(ppm) = 9.65 (br, 1H, H_a), 9.15 (d, 2H, H_b, ³*J*_{H-H} = 6.6 Hz), 9.01 (br, 1H, H_c), 7.60 (d, 1H, H_d, ³*J*_{H-H} = 9.0 Hz), 7.52 (dd, 1H, H_e, ³*J*_{H-H} = 9.0 Hz, ⁴*J*_{H-H} = 2.0 Hz), 7.40 (d, 2H, H_f, ³*J*_{H-H} = 6.6 Hz), 7.35 (d, 1H, H_g, ³*J*_{H-H} = 5.2 Hz), 1.59 (s, 15H, H_{h/h}), 1.55 (s, 15H, H_{h/h}); **¹³C{¹H} NMR (100 MHz, CDCl₃)**: δ(ppm) = 154.1, 148.5, 146.6, 145.6, 137.2, 131.2, 129.5, 126.5, 125.9, 125.0, 121.8, 86.5, 86.2, 9.2, 8.8; **IR (ATR)** (*ν*_{max}/cm⁻¹): 1607 (C=N_{py}), 1587 (C=N_{quin}); **M.P.** (°C): onset of decomp. with melting = 286.4; **HR-MS** (ESI (+), *m/z*): 483.1130 (17%, [M - 2Cl]²⁺), calculated 483.2480, 603.0919 (49%, [Ir₂C₂₄H₂₄Cl₂N₂]⁺), calculated 603.5960.

[{RuCl₂(*p*-cymene)₂(μ-L)], (**1d**). Ligand **L** (0.0449 g, 0.187 mmol) and [Ru(*p*-cymene)(μ-Cl)Cl]₂ (0.102 g, 0.167 mmol) yielded **1d** as a mustard powder. **Yield**: 74% (0.105 g, 0.123 mmol); **¹H NMR (300 MHz, CDCl₃)**: δ(ppm) = 9.24 (d, 2H, H_b, ³*J*_{H-H} = 6.2 Hz), 9.05 (br, 1H, H_a), 8.25 (br, 1H, H_c), 7.66 (d, 1H, H_d, ³*J*_{H-H} = 8.6 Hz), 7.52 (dd, 1H, H_e, ³*J*_{H-H} = 9.0 Hz, ⁴*J*_{H-H} = 1.7 Hz), 7.42 (br, 2H, H_f), 7.32 (d, 1H, H_g, ³*J*_{H-H} = 4.5 Hz), 5.54 (d, 2H, H_{h/h}, ³*J*_{H-H} = 5.7 Hz), 5.49 (d, 2H, H_{h/h}, ³*J*_{H-H} = 5.5 Hz), 5.35 (d, 4H, H_{i/i}, ³*J*_{H-H} = 5.5 Hz), 3.18–3.02 (m, 1H, H_{j/j}), 3.01–2.85 (m, 1H, H_{j/j}), 2.22 (s, 3H, H_{k/k}), 2.17 (s, 3H, H_{k/k}), 1.37 (d, 6H, H_{l/l}, ³*J*_{H-H} = 6.9 Hz), 1.29 (d, 6H, H_{l/l}, ³*J*_{H-H} = 6.9 Hz); **¹³C{¹H} NMR (100 MHz, CDCl₃)**: 155.4, 151.0, 149.0, 147.2, 144.0, 136.4, 129.2, 128.9, 126.2, 124.9, 123.8, 121.2, 104.2, 101.4, 97.4, 96.8, 82.8, 82.6, 81.4, 80.7, 30.9, 30.8, 22.5, 22.3, 19.0, 18.5; **IR (ATR)** (*ν*_{max}/cm⁻¹): 1608 (C=N_{py}), 1587 (C=N_{quin}); **M.P.** (°C): onset of decomp. with melting = 155.5; **HR-MS** (ESI (+), *m/z*): 390.9359 (19%, [M - 2Cl]²⁺), calculated 391.0900, 324.0395 (17%, [M - (*p*-cymene) - 2Cl]²⁺), calcu-

lated 323.9790, 511.0275 (55%, [RuC₂₄H₂₃Cl₂N₂]⁺), calculated 511.4380.

General procedure for the synthesis of metallarectangles (2c and 2d). Ag(CF₃SO₃) (2.1 eq.), in anhydrous acetonitrile, was added to a stirring solution of the appropriate *N,N'*-binuclear complex (**1c** or **1d**) (1 eq.) in dry CH₂Cl₂. The mixture was shielded from light and stirred at r.t. for 24 hours. The solvent was removed under reduced pressure, CH₂Cl₂ added to the remaining residue, and the solution filtered to remove the insoluble salts. The filtrate was concentrated and added to excess cold Et₂O, resulting in the precipitation of the corresponding metallarectangle, as its triflate salt.

[{Ir(μ-Cl)(Cp*)}₂(μ-L)₂](CF₃SO₃)₄, (**2c**). Ag(CF₃SO₃) (0.0219 g, 0.0852 mmol) in anhydrous acetonitrile (10.0 mL) was added to a solution of **1c** (0.0419 g, 0.0404 mmol) in dry CH₂Cl₂ (10.0 mL), yielding **2c** as a pale yellow powder. **Yield**: 71% (0.0365 g, 0.0144 mmol); **¹H NMR (300 MHz, [D₆]-DMSO)**: δ(ppm) = 9.12 (d, 2H, H_a, ³*J*_{H-H} = 4.4 Hz), 8.94 (d, 4H, H_b, ³*J*_{H-H} = 6.4 Hz), 8.25 (d, 2H, H_c, ⁴*J*_{H-H} = 2.1 Hz), 8.01 (d, 4H, H_f, ³*J*_{H-H} = 6.7 Hz), 7.97 (d, 2H, H_d, ³*J*_{H-H} = 9.1 Hz), 7.72 (dd, 2H, H_e, ³*J*_{H-H} = 9.0 Hz, ⁴*J*_{H-H} = 2.2 Hz), 7.69 (d, 2H, H_g, ³*J*_{H-H} = 4.4 Hz), 1.75 (s, 20H, H_{h/h}), 1.64 (s, 40H, H_{h/h}); **¹³C{¹H} NMR (100 MHz, [D₆]-DMSO)**: δ (ppm) = 153.9, 151.6, 148.4, 142.8, 134.7, 128.6, 128.3, 127.1, 123.1, 122.2, 121.7, 119.6, 100.4, 94.5, 8.6, 8.0; **IR (ATR)** (*ν*_{max}/cm⁻¹): 1609 (C=N_{py}), 1589 (C=N_{quin}), 1252 (CF₃ sym), 1222 (SO₃ asym), 1159 (CF₃ asym), 1029 (SO₃ sym); **M.P.** (°C): onset of decomp. without melting = 242.5; **HR-MS** (ESI (+), *m/z*): 483.2129 (48%, [M - 4OTf]⁴⁺), calculated 483.2490, 603.0921 (100%, [Ir₂C₄₈H₄₈N₄Cl₄]²⁺), calculated 603.596.

[{Ru(μ-Cl)(*p*-cymene)₂(μ-L)₂](CF₃SO₃)₄, (**2d**). Ag(CF₃SO₃) (0.0500 g, 0.195 mmol) in anhydrous acetonitrile (3.00 mL) was added to a solution of **1d** (0.0721 g, 0.0845 mmol) in dry CH₂Cl₂ (5.00 mL), yielding **2d** as an orange powder. **Yield**: 24% (0.0218 g, 0.0101 mmol); **¹H NMR (300 MHz, [D₆]-DMSO)**: δ(ppm) = 9.10 (d, 2H, H_a, ³*J*_{H-H} = 4.3 Hz), 8.97 (d, 4H, H_b, ³*J*_{H-H} = 6.4 Hz), 8.24 (d, 2H, H_c, ⁴*J*_{H-H} = 2.0 Hz), 7.94 (d, 4H, H_f, ³*J*_{H-H} = 7.0 Hz), 7.89–7.79 (m, 2H, H_d), 7.73 (dd, 2H, H_e, ³*J*_{H-H} = 9.0 Hz, ⁴*J*_{H-H} = 1.9 Hz), 7.76 (d, 2H, H_g, ³*J*_{H-H} = 4.3 Hz); **¹³C{¹H} NMR (100 MHz, [D₆]-DMSO)**: δ (ppm) = 153.9, 151.5, 148.4, 148.4, 142.8, 134.7, 128.5, 128.3, 127.1, 123.1, 122.3, 122.2, 119.1, 100.4, 94.5, 40.4, 8.6, 8.3, 7.9; **IR (ATR)** (*ν*_{max}/cm⁻¹): 1611 (C=N_{py}), 1589 (C=N_{quin}), 1244 (CF₃ sym), 1223 (SO₃ asym), 1156 (CF₃ asym), 1027 (SO₃ sym); **M.P.** (°C): onset of decomp. with melting = 120.4; **HR-MS** (ESI (+), *m/z*): 932.2568 (28%, [M - 2OTf]²⁺), calculated 932.2460, 1321.9711 (100%, [Ru₂C₄₈H₄₆Cl₄N₄]²⁺ (CF₃SO₃)₂), calculated 1321.0280.

General procedure for the synthesis of metallarectangles (3c and 3d). Ag(CF₃SO₃) (2.3 eq.) was added to a solution of either [{IrCl(Cp*)}₂(μ-η²-η²-C₂O₄)] or [{RuCl(*p*-cymene)₂(μ-η²-η²-C₂O₄)] (1 eq.), in anhydrous CH₃OH (10.0 mL), and the mixture stirred at r.t. for approximately 3 hours, ensuring complete abstraction of the chlorides. The AgCl was filtered by gravity and washed with anhydrous CH₃OH. Ligand **L** (1 eq.) was added to the filtrate and the mixture stirred for a final 24 hours. The solvent was removed under reduced pressure,



the residue suspended in CH_2Cl_2 , and the insoluble materials filtered. The filtrate was concentrated and added to excess cold Et_2O resulting in the precipitation of the corresponding metal-arectangles, as its triflate salt, in moderate yields.

$[\{\text{Ir}(\text{Cp}^*)\}_4(\mu\text{-}\eta^2\text{-}\eta^2\text{-C}_2\text{O}_4)(\mu\text{-L})_2](\text{CF}_3\text{SO}_3)_4$, (**3c**). $[\{\text{IrCl}(\text{Cp}^*)\}_2(\mu\text{-}\eta^2\text{-}\eta^2\text{-C}_2\text{O}_4)]$ (0.0500 g, 0.0614 mmol) was reacted with Ag (CF_3SO_3) (0.0387 g, 0.151 mmol), followed by **L** (0.0148 g, 0.0614 mmol), yielding **3c** as a mustard-yellow solid. **Yield**: 74% (0.0586 g, 0.0229 mmol); ^1H NMR (300 MHz, $[\text{D}_6]\text{-DMSO}$): δ (ppm) = 9.19–8.99 (m, 2H, H_a), 8.8–8.53 (m, 4H, H_b), 8.45–8.16 (m, 2H, H_c), 8.12–7.79 (m, 6H, $\text{H}_{f,d}$), 7.78–7.45 (m, 4H, $\text{H}_{e,g}$), 1.91–1.05 (m, 60H, $\text{H}_{h,h'}$); $^{13}\text{C}\{^1\text{H}\}$ NMR (100 MHz, $[\text{D}_6]\text{-DMSO}$): δ (ppm) = 165.0, 164.1, 152.2, 151.6, 148.4, 142.7, 134.8, 128.4, 127.0, 123.2, 122.3, 119.1, 115.9, 94.5, 93.9, 93.5, 90.9, 83.9, 8.3, 7.9; **IR** (ATR) ($\nu_{\text{max}}/\text{cm}^{-1}$): 1627 (C=O), 1250 (CF_3 sym), 1222 (SO_3 asym), 1155 (CF_3 asym), 1019 (SO_3 sym); **M.P.** ($^\circ\text{C}$): onset of decomp. without melting = 271.8; **HR-MS** (ESI (+), m/z): 492.0915 (32%, $[\text{M} - 4\text{OTf}]^{4+}$), calculated 491.8040; 1133.0420 (53%, $[\text{M} - 2\text{OTf}]^{2+}$), calculated 1132.6900, 717.0756 (95%, $[\text{IrC}_{24}\text{H}_{24}\text{N}_2\text{Cl}]^+(\text{CF}_3\text{SO}_3)^-$), calculated 717.2220.

$[\{\text{Ru}(p\text{-cymene})\}_4(\mu\text{-}\eta^2\text{-}\eta^2\text{-C}_2\text{O}_4)(\mu\text{-L})_2](\text{CF}_3\text{SO}_3)_4$, (**3d**). AgOTf (0.0685 g, 0.267 mmol), $[\{\text{RuCl}(p\text{-cymene})\}_2(\mu\text{-}\eta^2\text{-}\eta^2\text{-C}_2\text{O}_4)]$ (0.0700 g, 0.111 mmol) and **L** (0.0268 g, 0.111 mmol) yielded **3d** as a yellow solid. **Yield**: 71% (0.0867 g, 0.0395 mmol); ^1H NMR (300 MHz, $[\text{D}_6]\text{-DMSO}$): δ (ppm) = 9.11 (d, 2H, $\text{H}_{a/a'}$, $^3J_{\text{H-H}} = 4.4$ Hz), 9.05 (d, 2H, $\text{H}_{a/a'}$, $^3J_{\text{H-H}} = 4.3$ Hz), 8.81 (d, 4H, $\text{H}_{b/b'}$, $^3J_{\text{H-H}} = 6.3$ Hz), 8.66 (d, 4H, $\text{H}_{b/b'}$, $^3J_{\text{H-H}} = 6.3$ Hz), 8.26 (d, 2H, $\text{H}_{c/c'}$, $^3J_{\text{H-H}} = 1.8$ Hz), 8.22 (d, 2H, $\text{H}_{c/c'}$, $^3J_{\text{H-H}} = 2.0$ Hz), 7.90 (d, 4H, $\text{H}_{f/f'}$, $^3J_{\text{H-H}} = 6.4$ Hz), 7.83 (d, 4H, $\text{H}_{f/f'}$, $^3J_{\text{H-H}} = 6.5$ Hz), 7.77–7.67 (m, 4H, $\text{H}_{e,e'}$), 7.67–7.28 (m, 8H, $\text{H}_{d,d'}$, g,g'), 6.12 (d, 8H, $\text{H}_{h/h'}$, $^3J_{\text{H-H}} = 6.1$ Hz), 5.98 (d, 8H, $\text{H}_{h/h'}$, $^3J_{\text{H-H}} = 6.1$ Hz), 5.85 (d, 8H, $\text{H}_{i/i'}$, $^3J_{\text{H-H}} = 5.9$ Hz), 5.63 (d, 8H, $\text{H}_{i/i'}$, $^3J_{\text{H-H}} = 6.0$ Hz), 2.92–2.69 (m, 8H, $\text{H}_{j,j'}$), 2.30–1.99 (m, 24H, $\text{H}_{k,k'}$), 1.44–1.09 (m, 48H, $\text{H}_{l,l'}$); $^{13}\text{C}\{^1\text{H}\}$ NMR (100 MHz, $[\text{D}_6]\text{-DMSO}$): δ (ppm) = 172.4, 166.3, 164.4, 153.0, 151.6, 150.1, 148.4, 145.3, 145.0, 144.5, 143.1, 134.5, 128.8, 128.2, 128.0, 127.2, 126.1, 124.3, 123.8, 123.3, 121.8, 119.1, 102.7, 96.8, 80.4, 80.0, 33.0, 24.0, 21.9, 20.6; **IR** (ATR) ($\nu_{\text{max}}/\text{cm}^{-1}$): 1627 (C=O), 1251 (CF_3 sym), 1224 (SO_3 asym), 1152 (CF_3 asym), 1028 (SO_3 sym); **M.P.** ($^\circ\text{C}$): onset of decomp. without melting = 188.0; **HR-MS** (ESI (+), m/z): 949.0110 (43%, $[\text{M} - 2\text{OTf}]^{2+}$), calculated 948.3640, 425.9915 (57%, $[\text{Ru}_3\text{C}_{60}\text{H}_{60}\text{N}_4\text{O}_4\text{Cl}_2]^{3+}$), calculated 425.0967.

X-ray crystallography

Suitable single crystals of the iridium binuclear complex **1c** were grown by the slow evaporation of a saturated chloroform solution, at room temperature. Single-crystal X-ray diffraction data were collected on a Bruker KAPPA APEX II DUO diffractometer using graphite-monochromated Mo-K α radiation ($\lambda = 0.71073$ Å). Data collection was carried out at 100(2) K. The temperature was controlled by an Oxford Cryostream cooling system (Oxford Cryostat). Cell refinement and data reduction were performed using the program SAINT.⁹² The data were scaled and absorption correction performed using SADABS.⁹³ The structure was solved by direct methods using SHELXS-97⁹³ and refined by full-matrix least-squares methods based on F^2

using SHELXL-2018⁹³ and using the graphics interface program X-Seed.^{94,95} The programs X-Seed and POV-Ray were used to prepare molecular graphic images. All non-hydrogen atoms were refined anisotropically. All hydrogen atoms were placed in idealised positions and refined in riding models with U_{iso} assigned 1.2 or 1.5 times U_{eq} of their parent atoms and the bond distances were constrained to 0.95 Å, 0.98 Å, and 1.00 Å for different types of C–H.

DFT calculations

The structure of the model of the metallarectangle was predicted by density functional theory (DFT) calculations, using the DMol³ interface in BIOVIA Materials Studio 2017 (v. 17.1.0.48, 2016, Dassault Systèmes, Vélizy-Villacoublay Cedex, France).^{96–98} The molecular structure was optimized at the DFT level of theory, using the GGA-PBE density functional (*i.e.* generalized gradient approximation with Perdew–Burke–Ernzerhof exchange energies) and DND basis set (*i.e.* double numerical basis set with *d*-polarization functions (DND), file 4.4).⁹⁹ The quantum contributions of all electrons in the system were taken into consideration in the calculation. For quality of the calculation, the integration accuracy was set to coarse, with a SCF tolerance of 1.0×10^{-4} and a maximum number of 50 cycles. The spin polarization was restricted and a global orbital cut off set at 3.40 Å, with no solvation model, as the calculation was done *in vacuo*.

Biological methods

In vitro antiplasmodial assay. The test samples were evaluated in triplicate on two or three separate occasions against the chloroquine-sensitive (NF54) and chloroquine-resistant (K1) strains of *P. falciparum*. Continuous *in vitro* cultures of asexual erythrocyte stages of *P. falciparum* were maintained using a modified method of Trager and Jensen.¹⁰⁰ Quantitative assessment of antiplasmodial activity *in vitro* was determined via the parasite lactate dehydrogenase assay using a modified method described by Makler.¹⁰¹ The test samples were prepared to a 20 mg mL^{−1} stock solution in 100% DMSO and stored at -20 °C. Further dilutions were prepared on the day of the experiment. Chloroquine diphosphate (CQDP) was used as the reference drug in all experiments and was prepared to a 2 mg mL^{−1} stock solution in MilliQ water. Test samples were tested at a starting concentration of 100 $\mu\text{g mL}^{-1}$, which was then serially diluted 2-fold in complete medium to give 10 concentrations, with the lowest concentration being 0.2 $\mu\text{g mL}^{-1}$. The same dilution technique was used for all samples. A full dose–response was performed for all compounds to determine the concentration inhibiting 50% of parasite growth (IC_{50} value). The IC_{50} values were obtained using a non-linear dose–response curve fitting analysis via Graph Pad Prism v.5.0 software.

β -Haematin inhibition assay. The β -haematin inhibition assay was modified from the method described by Sandlin *et al.*^{85,86} Stock solutions (10 mM or 20 mM) of the respective test compounds were prepared in 100% DMSO, with the exception of CQDP, which was prepared in MilliQ water. The com-



pounds were dispensed into a 96-well plate in triplicate and were tested over a concentration range of 0–1000 μM or 0–500 μM (final well concentration). A 100 μL solution of MilliQ water/NP-40/DMSO in a v/v ratio of 7 : 2 : 1 was added to all wells in columns 1–11. MilliQ water (140 μL) and NP-40 (305.5 μM , 40.0 μL) was added to column 12. NP-40 is a detergent used to mediate the formation of β -haematin. The respective test compounds (20.0 μL) were then added to column 12 and serially diluted two-fold to give a total of 11 concentrations. Column 1 thus served as a blank containing no test compound. Since the compounds were coloured, the plates were pre-read at 405 nm. A 25 mM stock solution of haematin was then prepared by dissolving haemin in DMSO and sonicating for 1 minute. A 178.8 μL aliquot of this haematin stock solution was suspended in acetate buffer (20.0 mL, 1 M, pH 4.8) and 100 μL of this suspension added to each well. The plates were covered and incubated at 37 °C for 6 hours in an incubator. The assay was analysed using the pyridine-ferrochrome method developed by Egan and co-workers.⁸⁷ A solution of pyridine/MilliQ water/acetone/HEPES (2 M, pH 7.4) in a v/v ratio of 5 : 2 : 2 : 1 respectively, was prepared, and 32.0 μL of this solution added to each well, followed by acetone (60.0 μL) and mixed. The absorbance was recorded using a Thermo Scientific Multiscan GO plate reader at 405 nm. The IC_{50} values were obtained using a sigmoidal dose-response curves generated using Graph Pad Prism v.5.0 software.

Conflicts of interest

There are no conflicts of interest to declare.

Acknowledgements

Financial support from the University of Cape Town and the National Research Foundation of South Africa (UID: 129288) is gratefully acknowledged. Dr Dale Taylor (H3D), Mr Virgil Verhoog and Mrs Sumaya Salie from the Department of Clinical Pharmacology (University of Cape Town) are gratefully acknowledged for their assistance with the pLDH assays. Professor Timothy Egan and Dr Roxanne Mohunlal from the Department of Chemistry (University of Cape Town) are also gratefully acknowledged for their assistance with the β -haematin inhibition studies.

References

- 1 <https://www.who.int/news-room/feature-stories/detail/world-malaria-report-2019>.
- 2 P. F. Salas, C. Herrmann and C. Orvig, *Chem. Rev.*, 2013, **113**, 3450–3492.
- 3 R. Carter and K. N. Mendis, *Clin. Microbiol. Rev.*, 2002, **15**, 564–594.
- 4 M. Navarro, C. Gabbiani, L. Messori and D. Gambino, *Drug Discovery Today*, 2010, **15**, 1070–1078.
- 5 L. Tilley, P. Loria and M. Foley, *Antimalarial Chemotherapy*, Humana Press Inc., Totowa, New Jersey, 2001.
- 6 R. A. Jones, S. S. Panda and C. D. Hall, *Eur. J. Med. Chem.*, 2015, **97**, 335–355.
- 7 *Guidelines for the treatment of malaria*, WHO report, <http://helid.digicollection.org/pdf/s13418e/s13418e.pdf>, 2006.
- 8 *Guidelines for the treatment of malaria*, WHO report, https://www.who.int/docs/default-source/documents/publications/gmp/guidelines-for-the-treatment-of-malaria-eng.pdf?sfvrsn=a0138b77_2, 2015.
- 9 Y. Bansal and O. Silakari, *Eur. J. Med. Chem.*, 2014, **76**, 31–42.
- 10 E. A. Ashley, M. Dhorda, R. M. Fairhurst, C. Amarutunga, P. Lim, S. Suon, S. Sreng, J. M. Anderson, S. Mao, B. Sam, C. Sopha, C. M. Chuor, C. Nguon, S. Sovannaroth, S. Pukrittayakamee, P. Jittamala, K. Chotivanich, K. Chutasmit, C. Suchatsoonthorn, R. Runcharoen, T. T. Hien, N. T. Thuy-Nhien, N. V. Thanh, N. H. Phu, Y. Htut, K.-T. Han, K. H. Aye, O. A. Mokuolu, R. R. Olaosebikan, O. O. Folaranmi, M. Mayxay, M. Khanthavong, B. Hongvanthong, P. N. Newton, M. A. Onyamboko, C. I. Fanello, A. K. Tshefu, N. Mishra, N. Valecha, A. P. Phyto, F. Nosten, P. Yi, R. Tripura, S. Borrmann, M. Bashraheil, J. Peshu, M. A. Faiz, A. Ghose, M. A. Hossain, R. Samad, M. R. Rahman, M. M. Hasan, A. Islam, O. Miotto, R. Amato, B. MacInnis, J. Stalker, D. P. Kwiatkowski, Z. Bozdech, A. Jeeyapant, P. Y. Cheah, T. Sakulthaew, J. Chalk, B. Intharabut, K. Silamut, S. J. Lee, B. Vihokhern, C. Kunasol, M. Imwong, J. Tarning, W. J. Taylor, S. Yeung, C. J. Woodrow, J. A. Flegg, D. Das, J. Smith, M. Venkatesan, C. V. Plowe, K. Stepniewska, P. J. Guerin, A. M. Dondorp, N. P. Day and N. J. White, *N. Engl. J. Med.*, 2014, **371**, 411–423.
- 11 W. Sim, R. T. Barnard, M. A. T. Blaskovich and Z. M. Ziora, *Antibiotics*, 2018, **7**, 1–15.
- 12 S. Medici, M. Peana, G. Crisponi, V. M. Nurchi, J. I. Lachowicz, M. Remelli and M. A. Zoroddu, *Coord. Chem. Rev.*, 2016, **327–328**, 349–359.
- 13 G. Faa, C. Gerosa, D. Fanni, J. I. Lachowicz and V. M. Nurchi, *Curr. Med. Chem.*, 2018, **25**, 75–84.
- 14 S. Dilruba and G. V. Kalayda, *Cancer Chemother. Pharmacol.*, 2016, **77**, 1103–1124.
- 15 Z. Guo and P. J. Sadler, *Angew. Chem., Int. Ed.*, 1999, **38**, 1512–1531.
- 16 L. Kelland, *Nat. Rev. Cancer*, 2007, **7**, 573–584.
- 17 U. Schatzschneider, in *Advances in Bioorganometallic Chemistry*, ed. T. Hirao and T. Moriuchi, Elsevier Inc., 1st edn, 2019, pp. 173–192.
- 18 J. Held, C. Supan, C. L. O. Salazar, H. Tinto, L. N. Bonkian, A. Nahum, B. Moulero, A. Sié, B. Coulibaly, S. B. Sirima, M. Siribie, N. Otsyula, L. Otieno, A. M. Abdallah, R. Kimutai, M. Bouyou-Akotet, M. Kombila, K. Koiwai, C. Cantalloube, C. Din-Bell, E. Djeriou, J. Waitumbi, B. Mordmüller, D. Ter-Minassian, B. Lell and P. G. Kremsner, *Lancet Infect. Dis.*, 2015, **15**, 1409–1419.



- 19 T. R. Cook, Y. R. Zheng and P. J. Stang, *Chem. Rev.*, 2013, **113**, 734–777.
- 20 W. X. Gao, H. J. Feng, B. B. Guo, Y. Lu and G. X. Jin, *Chem. Rev.*, 2020, **120**, 6288–6325.
- 21 J.-Q. Wang, C.-X. Ren and G.-X. Jin, *Organometallics*, 2006, **25**, 74–81.
- 22 Y. F. Han, W. G. Jia, W. B. Yu and G. X. Jin, *Chem. Soc. Rev.*, 2009, **38**, 3419–3434.
- 23 Y. F. Han, W. G. Jia, Y. J. Lin and G. X. Jin, *Organometallics*, 2008, **27**, 5002–5008.
- 24 Y. Han and G. Jin, *Acc. Chem. Res.*, 2014, **47**, 3571–3579.
- 25 L. L. Ma, J. Q. Han, W. G. Jia and Y. F. Han, *Beilstein J. Org. Chem.*, 2018, **14**, 2027–2034.
- 26 J. Mattsson, P. Govindaswamy, A. K. Renfrew, P. J. Dyson, P. Stepnicka, B. Süss-Fink and B. Therrien, *Organometallics*, 2009, **28**, 4350–4357.
- 27 A. Dubey, J. W. Min, H. J. Koo, H. Kim, T. R. Cook, S. C. Kang, P. J. Stang and K. W. Chi, *Chem. – Eur. J.*, 2013, **19**, 11622–11628.
- 28 G. L. Wang, Y. J. Lin and G. X. Jin, *J. Organomet. Chem.*, 2010, **695**, 1225–1230.
- 29 Y. F. Han, Y. J. Lin, W. G. Jia and G. X. Jin, *Organometallics*, 2008, **27**, 4088–4097.
- 30 Y.-F. Han, Y.-J. Lin, W.-G. Jia, L.-H. Weng and G.-X. Jin, *Organometallics*, 2007, **26**, 5848–5853.
- 31 R. Chakrabarty, P. S. Mukherjee and P. J. Stang, *Chem. Rev.*, 2011, **111**, 6810–6918.
- 32 B. J. Holliday and C. A. Mirkin, *Angew. Chem., Int. Ed.*, 2001, **40**, 2022–2043.
- 33 B. Therrien, *Eur. J. Inorg. Chem.*, 2009, **2009**, 2445–2453.
- 34 Y. Yamamotoa, H. Suzuki, N. Tajima and K. Tatsumi, *Chem. – Eur. J.*, 2002, **8**, 372–379.
- 35 K. Severin, *Chem. Commun.*, 2006, 3859–3867.
- 36 T. R. Cook, V. Vajpayee, M. H. Lee, P. J. Stang and K. Chi, *Acc. Chem. Res.*, 2013, **46**, 2464–2474.
- 37 H. N. Zhang, Y. J. Lin and G. X. Jin, *J. Am. Chem. Soc.*, 2021, **143**, 1119–1125.
- 38 P. F. Cui, Y. J. Lin, Z. H. Li and G. X. Jin, *J. Am. Chem. Soc.*, 2020, **142**, 8532–8538.
- 39 Y. Lu, D. Liu, Y.-J. Lin, Z.-H. Li and G.-X. Jin, *Natl. Sci. Rev.*, 2020, **7**, 1548–1556.
- 40 C. Y. Zhu, M. Pan and C. Y. Su, *Isr. J. Chem.*, 2018, **59**, 209–219.
- 41 Y. F. Han, H. Li and G. X. Jin, *Chem. Commun.*, 2010, **46**, 6879–6890.
- 42 J. Mattsson, P. Govindaswamy, J. Furrer, Y. Sei, K. Yamaguchi, B. Süss-Fink and B. Therrien, *Organometallics*, 2008, **27**, 4346–4356.
- 43 N. P. E. Barry and B. Therrien, *Eur. J. Inorg. Chem.*, 2009, **2009**, 4695–4700.
- 44 B. Therrien, G. Süss-Fink, P. Govindaswamy, A. K. Renfrew and P. J. Dyson, *Angew. Chem., Int. Ed.*, 2008, **47**, 3773–3776.
- 45 J. Mattsson, O. Zava, A. K. Renfrew, Y. Sei, K. Yamaguchi, P. J. Dyson and B. Therrien, *Dalton Trans.*, 2010, **39**, 8248–8255.
- 46 N. P. E. Barry, O. Zava, P. J. Dyson and B. Therrien, *Chem. – Eur. J.*, 2011, **17**, 9669–9677.
- 47 A. Casini, B. Woods and M. Wenzel, *Inorg. Chem.*, 2017, **56**, 14715–14729.
- 48 S. L. Huang, Y. J. Lin, T. S. Hor and G. X. Jin, *J. Am. Chem. Soc.*, 2013, **135**, 8125–8128.
- 49 N. P. Barry, F. Edeaf and B. Therrien, *Dalton Trans.*, 2011, **40**, 7172–7180.
- 50 V. Vajpayee, Y. J. Yang, S. C. Kang, H. Kim, I. S. Kim, W. Ming, P. J. Stang and K. W. Chi, *Chem. Commun.*, 2011, **47**, 5184–5186.
- 51 H. S. Song, Y. H. Song, N. Singh, H. Kim, H. Jeon, I. Kim, S. C. Kang and K.-W. Chi, *Sci. Rep.*, 2019, **9**, 1–13.
- 52 H. Vardhan, A. Nafady, A. M. Al-Enizi, K. Khandker, H. M. El-Sagher, G. Verma, M. Acevedo-Duncan, T. M. Alotaibi and S. Ma, *Molecules*, 2019, **24**, 2284.
- 53 G. Gupta, A. Das, S. W. Lee, J. Y. Ryu, J. Lee, N. Nagesh, N. Mandal and C. Y. Lee, *J. Organomet. Chem.*, 2018, **868**, 86–94.
- 54 G. Gupta, A. Das, J. Lee, N. Mandal and C. Y. Lee, *ChemPlusChem*, 2018, **83**, 339–347.
- 55 G. Gupta, B. S. Murray, P. J. Dyson and B. Therrien, *Materials*, 2013, **6**, 5352–5366.
- 56 G. Gupta, J. M. Kumar, A. Garci, N. Nagesh and B. Therrien, *Molecules*, 2014, **19**, 6031–6046.
- 57 A. Pothig and A. Casini, *Theranostics*, 2019, **9**, 3150–3169.
- 58 Y. Zhao, L. Zhang, X. Li, Y. Shi, R. Ding, M. Teng, P. Zhang, C. Cao and P. J. Stang, *Proc. Natl. Acad. Sci. U. S. A.*, 2019, **116**, 4090–4098.
- 59 A. Mishra, S. C. Lee, N. Kaushik, T. R. Cook, E. H. Choi, N. K. Kaushik, P. J. Stang and K. W. Chi, *Chem. – Eur. J.*, 2014, **20**, 14410–14420.
- 60 Y. R. Zheng, K. Suntharalingam, P. M. Bruno, W. Lin, W. Wang, M. T. Hemann and S. J. Lippard, *Inorg. Chim. Acta*, 2016, **452**, 125–129.
- 61 S. M. McNeill, D. Preston, J. E. Lewis, A. Robert, K. Knerr-Rupp, D. O. Graham, J. R. Wright, G. I. Giles and J. D. Crowley, *Dalton Trans.*, 2015, **44**, 11129–11136.
- 62 Z. Yue, H. Wang, Y. Li, Y. Qin, L. Xu, D. J. Bowers, M. Gangoda, X. Li, H. B. Yang and Y. R. Zheng, *Chem. Commun.*, 2018, **54**, 731–734.
- 63 N. P. Barry, F. Edeaf, P. J. Dyson and B. Therrien, *Dalton Trans.*, 2010, **39**, 2816–2820.
- 64 A. Casini and J. D. Crowley, *Front. Chem.*, 2019, **7**, 293.
- 65 H. Sepehrpour, W. Fu, Y. Sun and P. J. Stang, *J. Am. Chem. Soc.*, 2019, **141**, 14005–14020.
- 66 N. Kudo, M. Perseghini and G. C. Fu, *Angew. Chem., Int. Ed.*, 2006, **45**, 1282–1284.
- 67 P. Govindaswamy, G. Süss-Fink and B. Therrien, *Organometallics*, 2007, **26**, 915–924.
- 68 E. H. Wi, J. Y. Ryu, S. G. Lee, U. Farwa, M. Pait, S. Lee, S. Cho and J. Lee, *Inorg. Chem.*, 2019, **58**, 11493–11499.
- 69 P. Govindaswamy, G. Süss-Fink and B. Therrien, *Inorg. Chem. Commun.*, 2007, **10**, 1489–1492.
- 70 B. Therrien, *Coord. Chem. Rev.*, 2009, **253**, 493–519.



- 71 E. Ekengard, K. Kumar, T. Fogeron, C. de Kock, P. J. Smith, M. Haukka, M. Monarid and E. Nordlander, *Dalton Trans.*, 2016, **45**, 3905–3917.
- 72 P. Chellan, K. M. Land, A. Shokar, A. Au, S. H. An, D. Taylor, P. J. Smith, K. Chibale and G. S. Smith, *Organometallics*, 2013, **32**, 4793–4804.
- 73 K.-G. Liu, X.-Q. Cai, X.-C. Li, D.-A. Qin and M.-L. Hu, *Inorg. Chim. Acta*, 2012, **388**, 78–83.
- 74 D. C. Caskey, T. Yamamoto, C. Addicott, R. K. Shoemaker, J. Vacek, A. M. Hawkridge, D. C. Muddiman, G. S. Kottas, J. Michl and P. J. Stang, *J. Am. Chem. Soc.*, 2008, **130**, 7620–7628.
- 75 L. Tilley, P. Loria and M. Foley, in *Antimalarial Chemotherapy*, ed. P. J. Rosenthal, Humana Press Inc., Totowa, NJ, 2001, pp. 87–121.
- 76 S. K. Singh and S. Singh, *Int. J. Pharm. Sci. Rev. Res.*, 2014, **25**, 295–302.
- 77 R. A. Sánchez-Delgado, M. Navarro, H. Pérez and J. A. Urbina, *J. Med. Chem.*, 1996, **39**, 1095–1099.
- 78 C. S. K. Rajapakse, A. Martínez, B. Naoulou, A. A. Jarzecki, L. Suárez, C. Deregnacourt, V. Sinou, J. Schrével, E. Musi, G. Ambrosini, G. K. Schwartz and R. A. Sánchez-Delgado, *Inorg. Chem.*, 2009, **48**, 1122–1131.
- 79 D. R. Melis, C. B. Barnett, L. Wiesner, E. Nordlander and G. S. Smith, *Dalton Trans.*, 2020, **49**, 11543–11555.
- 80 D. E. Goldberg, A. F. G. Slater, A. Cerami and G. B. Henderson, *Proc. Natl. Acad. Sci. U. S. A.*, 1990, **87**, 2931–2935.
- 81 S. E. Francis, J. David, J. Sullivan and D. E. Goldberg, *Annu. Rev. Microbiol.*, 1997, **51**, 97–123.
- 82 M. Navarro, W. Castro and C. Biot, *Organometallics*, 2012, **31**, 5715–5727.
- 83 M. Mushtaque and Shahjahan, *Eur. J. Med. Chem.*, 2015, **90**, 280–295.
- 84 M. Foley and L. Tilley, *Pharmacol. Ther.*, 1998, **79**, 55–87.
- 85 R. D. Sandlin, M. D. Carter, P. J. Lee, J. M. Auschwitz, S. E. Leed, J. D. Johnson and D. W. Wright, *Antimicrob. Agents Chemother.*, 2011, **55**, 3363–3369.
- 86 M. D. Carter, V. V. Phelan, R. D. Sandlin, B. O. Bachmann and D. W. Wright, *Comb. Chem. High Throughput Screening*, 2010, **13**, 285–292.
- 87 K. K. Ncokazi and T. J. Egan, *Anal. Biochem.*, 2005, **338**, 306–319.
- 88 C. White, A. Yates and P. M. Maitlis, in *Inorganic Syntheses*, ed. D. M. Heinekey, John Wiley & Sons Inc., 1992, vol. 29, ch. 53, pp. 228–234.
- 89 M. A. Bennet, T.-N. Huang, T. W. Matheson and A. K. Smith, in *Inorganic Syntheses*, ed. S. Ittel and W. Nickerson, John Wiley & Sons Inc., 1982, vol. XXI, ch. 16, pp. 75–78.
- 90 H. Yan, G. Süss-Fink, A. Neels and H. Stoeckli-Evans, *Dalton Trans.*, 1997, 4345–4350.
- 91 A. Bacchi, G. Cantoni, P. Pelagatti and S. Rizzato, *J. Organomet. Chem.*, 2012, **714**, 81–87.
- 92 SAINT, Version 7.60a, Bruker AXS Inc., Madison, WI, USA, 2006.
- 93 G. M. Sheldrick, *SHELXS-97, SHELXL-2018/3 and SADABS version 2.05*, University of Göttingen, Germany, 1997.
- 94 L. J. Barbour, *J. Supramol. Chem.*, 2001, **1**, 189–191.
- 95 J. L. Atwood and L. J. Barbour, *Cryst. Growth Des.*, 2003, **3**, 3–8.
- 96 B. Delley, *J. Chem. Phys.*, 1990, **92**, 508–517.
- 97 B. Delley, *J. Chem. Phys.*, 2000, **113**, 7756–7764.
- 98 BIOVIA Materials Studio, <https://www.materials-studio.com/products/collaborative-science/biovia-materials-studio>, accessed: 07 Dec 2020.
- 99 J. P. Perdew, J. A. Chevary, S. H. Vosko, K. A. Jackson, M. R. Pederson, D. J. Singh and C. Fiolhais, *Phys. Rev. B: Condens. Matter Mater. Phys.*, 1992, **46**, 6671–6687.
- 100 W. Trager and J. Jensen, *Science*, 1976, **193**, 673–675.
- 101 M. T. Makler and D. J. Hinrichs, *Am. J. Trop. Med. Hyg.*, 1993, **48**, 205–210.

